

## Material-independent crack arrest statistics: Application to indentation experiments

Yann Charles<sup>1,2</sup>, François Hild<sup>1\*</sup>, Stéphane Roux<sup>3</sup>, Damien Vandembroucq<sup>3</sup>

<sup>1</sup> LMT-Cachan, ENS de Cachan / CNRS-UMR 8535 / Université Paris 6  
61 avenue du Président Wilson, F-94235 Cachan Cedex, France.

<sup>2</sup> Now at GEMPPM, INSA-Lyon / CNRS-UMR 5510  
20 avenue Albert Einstein, F-69621 Villeurbanne Cedex, France.

<sup>3</sup> Unité Mixte CNRS/Saint-Gobain, Surface du Verre et Interfaces  
39 quai Lucien Lefranc, F-93303 Aubervilliers Cedex, France.

The date of receipt and acceptance will be inserted by the editor

**Abstract** An extensive experimental study of indentation and crack arrest statistics is presented for four different brittle materials (alumina, silicon carbide, silicon nitride, glass). Evidence is given that the crack length statistics is described by a universal (*i.e.*, material independent) distribution. The latter directly derives from results obtained when modeling crack propagation as a depinning phenomenon. Crack arrest (or effective toughness) statistics appears to be fully characterized by two parameters, namely, an asymptotic crack length (or macroscopic toughness) value and a power law size dependent width. The experimental knowledge of the crack arrest statistics at one given scale thus gives access to its knowledge at all scales.

**Key words** Brittle fracture, Crack arrest, Heterogeneity, Depinning, Indentation, Probability and statistics.

---

\* to whom correspondence should be addressed. Email: hild@lmt.ens-cachan.fr,  
Fax: +33 1 47 40 22 40.

## 1 Introduction

Indentation tests are widely used to estimate material properties such as hardness and toughness. These tests are local and non destructive. The application on the surface of a diamond pyramid with a force  $F$  creates an irreversible mark for any type of material and a network of cracks for brittle solids [Lawn, 1993] whose shape and direction depend on the tip geometry (Knoop, Vickers, Berkovich – see Fig. 1 for a Vickers indenter). The projected area  $A$  of the permanent print defines the Meyer hardness  $H = F/A$ . The toughness measurement mainly relies on the existence on an intermediate scaling law between the stress intensity factor (SIF)  $K$  and the length  $c$  of the cracks generated during the test  $K \propto F/c^{3/2}$  with a geometry and material dependent prefactor. This scaling is easily recovered in the framework of linear elastic fracture mechanics. Assuming a point force  $F$  (thus a stress field  $F/r^2$ ), the elastic energy released in a volume  $c^3$  due to the presence of radial cracks of radius  $c$  is estimated to be  $F^2/Ec$ . The energy release rate associated with a surface increase  $dS \propto cdc$  is thus  $G = K^2/E \propto F^2/Ec^3$  so that  $K \propto F/c^{3/2}$ .

The propagation being stable, the indentation cracks are arrested for a length such that the SIF equals the toughness  $K = K_c$ . Simple dimensional analysis shows that the above scaling holds when the plastic strain is neglected. However, even when plasticity is considered a similar scaling may hold. Lawn et al. [1980] used a plastic cavity model to estimate the residual stresses induced by indentation and proposed the following estimate for the toughness

$$K_c = \chi_R \frac{F}{c^{3/2}}, \quad \chi_R = \xi_0 (\cot \Phi)^{2/3} \sqrt{\frac{E}{H}}$$

where  $E$  and  $H$  are respectively the Young's modulus and the hardness, and  $\Phi$  is the half-angle of the indenter. Last,  $\xi_0$  is a dimensionless constant that remains slightly dependent on the plastic constitutive law of the material. Ample experimental data show that for large loads, such a scaling relation between  $F$  and  $c$  holds [Ponton and Rawlings, 1989a]. In the case of a Vickers indentation, one usually considers that this is the case for radial cracks for which  $c/a > 2$ , where  $a$  is the half diagonal of the plastic mark and  $c$  is the crack length. For smaller cracks, (*i.e.*, for smaller  $c/a$  ratio) deviations are systematically observed, but among the long list of proposed relations [Ponton and Rawlings, 1989a] between  $F$  and  $c$  no general conclusions are derived in this regime. Note that for such lengths, possible Palmqvist (or lateral) cracks may have been generated.

A key question has been raised in particular by Cook et al. [1985]. Is it valid to extrapolate the toughness value obtained at a microscopic scale with the indentation test to the large scale of macroscopic cracks? One limitation that is easily be foreseen is the effect of microstructure. At a small scale, the heterogeneous nature of the material may give rise to a local toughness variability (*e.g.*, nature of the phases, orientation of grains, grain boundaries, intrinsic heterogeneity). What will be the macroscopic

consequences of such a variability? A phenomenological approach to this question consists in introducing the so-called  $R$ -curve effect, where the apparent toughness depends explicitly on the crack length. Cook et al. [1985] proposed to introduce a shielding effect at the scale of the microstructure to give a phenomenological account to this phenomenon.

Beyond this systematic size effect, the local disorder induces a statistical scatter of the toughness measurements. Such a statistical scatter is well known in the context of strength measurements [Weibull, 1939] and appears at the initiation step. The fluctuations thus reflect the defect distribution within the material [Jayatilaka and Trustrum, 1977], especially at its surface for glass [Kurkjian, 1985]. In the case of indentation with a sharp tip, initiation usually takes place below the surface on defects which are either structural or induced by the plastic deformation.

The propagation being stable *i.e.*, the SIF at the crack tip decreases with  $c$  thus the crack stops as soon as the SIF is less than or equal to the toughness. In cases of large cracks and easy initiation, the scatter on toughness measurements is thus considered as independent of the initiation step and directly induced by the effect of the microstructural disorder on the crack arrest. Note however that a delayed or late initiation step due for instance to a very homogeneous material and defect free surface may be responsible for an additional scatter (this is especially the case for monocrystals where the crack propagation and arrest may result from elasto-dynamic effects after an initiation step that would allow for a large elastic energy being stored at the onset of fracture). The present study only focuses on the effect of microscopic disorder on the toughness measurements statistics in a quasi-static regime.

Though not directly in the context of indentation, the recent years have seen a growing interest for the study of fracture in heterogeneous materials [Herrmann and Roux, 1990]. It appears that many results obtained in the simple framework of the propagation of a plane crack is applied in the more complex case of the indentation geometry. Historically, the apparent universality of the scaling law characterizing the roughness of crack surfaces [Bouchaud, 1997] has motivated the use of models initially developed in the Statistical Physics community. The physics of a crack front arrested by an array of obstacles [Gao and Rice, 1989] is very similar to the one of a triple contact line in wetting experiments [Joanny and de Gennes, 1984] and is described as a depinning transition [Schmittbuhl et al., 1995]. In recent papers such depinning models were used i) to estimate the dependence of the macroscopic toughness on the details of the microscopic disorder [Roux et al., 2003] and ii) to propose a material independent description of the indentation crack arrest statistics [Charles et al., 2004].

It appears in particular that a precise description of the distribution of the toughness effectively “seen” by a front of extension  $L$  propagating through a heterogeneous material characterized by a toughness disorder at the microscopic scale  $\xi$  is obtained. Independently of the details of the microscopic disorder, this effective toughness distribution  $p(K_c, L/\xi)$  is char-

acterized by a universal functional form depending on two parameters only, namely, an asymptotic toughness  $K^*$  and the standard deviation  $\Sigma$  of an effective toughness distribution

$$p\left(K_c, \frac{L}{\xi}\right) = \psi\left(\frac{K^* - K_c}{\Sigma}\right)$$

where  $K^*$  is an intrinsic (constant) parameter of the material while  $\Sigma$  is size dependent,  $\Sigma = \Sigma_0(L/\xi)^{-1/\nu}$  depends only on the standard deviation  $\Sigma_0$  of the microscopic toughness distribution and on the relative length of the front  $L/\xi$ ,  $\nu$  being here a non trivial universal exponent [Skoe et al., 2002]. For crack fronts of infinite extension, the distribution converges toward a Dirac distribution at the macroscopic toughness value  $K^*$ . For all forms of microscopic toughness distribution, the statistical distribution of the ‘‘mesoscopic’’ toughness will follow the above universal form with a unique function  $\psi$  as soon as  $L/\xi \gg 1$ . This result is adapted to the specific case of indentation, and henceforth it will give rise to a universal form of the crack arrest length distribution [Charles et al., 2004].

The aim of the present paper is to test the validity of the latter predictions on a series of indentation experiments on various brittle materials (glass, alumina, silicon carbide and silicon nitride). The paper is organized as follows. The statistical modeling of crack pinning is briefly introduced and adapted to indentation. After presenting the experimental material and methods, the experimental results concerning the statistics of crack lengths at various load levels are analyzed within the previous theoretical framework.

## 2 Summary of the propagation model

A semi-infinite mode-I crack in an infinite medium propagating along a weak heterogeneous and virtual interface is considered. The heterogeneity is modeled by a random field of local toughness, with a small-scale correlation length  $\xi$  above which correlations are neglected. As the system is loaded by external forces up to the onset of crack propagation, the crack front does not remain straight, but rather displays corrugations so as to adjust the local SIF to the facing toughness. The difficulty of the problem essentially arises from the coupling between the crack front morphology,  $h(x)$  and the local SIF,  $K(x)$ . The latter is taken into account through the first order perturbation computation [Gao and Rice, 1989]

$$K(x) = K_0 \left( 1 + \frac{1}{\pi} \int_{-\infty}^{\infty} \frac{h(x) - h(x')}{(x - x')^2} dx' \right) \quad (1)$$

where  $K_0$  is the SIF that would be obtained in similar loading conditions for a straight crack front. Let us simply list here the main results concerning this model as obtained in previous studies [Skoe et al., 2002; Roux et al.,

2003]. For small disorder amplitude, small system size, and/or long correlation length of the toughness along the crack propagation direction, a regime of “weak pinning” is encountered where the crack front has a smooth change, and the macroscopic toughness is simply equal to the geometrical average of the local toughness. More interestingly, the most common situation, *i.e.*, the generic one for a large system as compared to the heterogeneity scale, is a regime of “strong pinning”. The latter is a second order phase transition where the control parameter is the macroscopic stress intensity factor. The critical point corresponds to the macroscopic toughness below which crack propagation is arrested and above which it is sustained forever. This criticality of the crack propagation onset comes along with standard features of second-order phase transitions such as the absence of characteristic length scales, self-similarity, scaling with universal critical exponents, a set of properties that are exploited in the sequel.

One of the first characteristic features is the occurrence of a correlated roughness of the crack front morphology with a long range correlation. The absence of length scale imposes a self-affine roughness where the front  $h(x)$  remains statistically invariant in the affine transformation  $x \rightarrow \lambda x$ ;  $h \rightarrow \lambda^\zeta h$ . The roughness or Hurst exponent,  $\zeta$ , is one critical exponent whose value — determined from numerical simulations — amounts to  $\zeta \approx 0.39$  [Rosso and Krauth, 2002; Vandembroucq and Roux, 2004]. The global roughness

$$w(L) = (\langle h(x)^2 \rangle - \langle h(x) \rangle_L^2)^{1/2} \quad (2)$$

therefore scales with the system size as  $w(L) \propto L^\zeta$ . Note that experimental roughness measurements on interfacial propagating fronts were shown to exhibit a self-affine character with a roughness exponent  $\zeta \approx 0.5 - 0.6$  Schmittbuhl and Måløy [1995] larger than the above numerical value  $\zeta \approx 0.39$ . In the following we use the latter value in order to test the validity of our model on experimental data.

The statistical distribution of *instantaneous* depinning force is non-universal. It reflects both the crack front morphology and the statistical distribution of local toughness. However, the depinning is organized in space and time in such a way that the front advance proceeds by a series of unstable jumps from one stable configuration to the next with a large (scale free, and hence power law) statistical distribution of such avalanches. The latter displays a hierarchical structure consisting of embedded sub-avalanches with a self-similar statistical distribution. The interesting feature is that the statistical distribution of depinning forces or toughness  $K_c$ ,  $p(K_c, \ell)$ , conditioned by the avalanche size (or more precisely by a characteristic distance  $\ell$  along the crack front) obeys some important scaling properties:

- The most important, is that as  $\ell$  tends to infinity, the distribution tends to a Dirac distribution

$$p(K_c, \ell) \longrightarrow \delta(K_c - K^*) \quad (3)$$

where  $K^*$  is the thermodynamic limit of the toughness. It is thus retrieved that for an infinite system size (relative to the size of the heterogeneities along the interface) the system converges toward a homogeneous one characterized by a deterministic toughness  $K^*$ .

- The way the convergence toward this deterministic limit occurs is further characterized. For a finite characteristic length scale  $\ell$ , the distribution  $p(K_c, \ell)$  has a standard deviation  $\Sigma(\ell) = (\langle K_c^2 \rangle - \langle K_c \rangle^2)^{1/2}$  that vanishes for diverging  $\ell$  as

$$\Sigma(\ell) \propto \Sigma_0 \left( \frac{\ell}{\xi} \right)^{-1/\nu} \quad (4)$$

where  $\nu = 1/(1 - \zeta) \approx 1.64$  is a universal exponent. Moreover, these two moments are sufficient to characterize the entire force distribution.

- The reduced toughness defined as  $u = (K^* - K_c)(\ell/\xi)^{1/\nu}$  is observed (for large  $\ell$ ) to follow a universal distribution

$$p(K_c, \ell) = \left( \frac{\ell}{\xi} \right)^{1/\nu} \psi(u) \quad (5)$$

where  $\psi$  is universal, that is  $\ell$ -independent, but more importantly also independent of the details of the local toughness distribution. In the above definition,  $\psi$  is defined at the scale  $\xi$  of the microscopic disorder, its shape is universal and its variance is equal to  $\Sigma_0^2$ , which is the only relevant microscopic parameter. For small arguments  $u \ll 1$ ,  $\psi(u)$  behaves as a power law

$$\psi(u) \approx A_0 \frac{u^\beta}{\Sigma_0^{\beta+1}} \quad (6)$$

where  $A_0$  is a constant of the order of unity and  $\beta = \zeta/(1 - \zeta) \approx 0.64$  is again a critical exponent. For large arguments  $\psi$  decays sharply to 0 (*i.e.*, faster than any power law).

- However, the record in time of the macroscopic toughness displays long range time correlations, which forbid all practical use of the above result without resorting to a more detailed study. These correlations are however exhausted past a characteristic propagation distance that exactly matches the front roughness. The condition for negligible correlations in the crack propagation is that the crack front has been renewed over its entire extension. Thus for a system size  $L$ , the distribution  $p(K_c, \ell = L)$  both displays the universal shape given by  $\psi$ , and the absence of correlations along the crack propagation axis which makes the information exploitable and useful.

It is highly non trivial that only two parameters  $K^*$  and  $\Sigma$  (for a reference scale  $L$ ) are sufficient to account for the entire distribution for any statistical distribution of local toughness. Using cautiously a loose analogy, this behavior is reminiscent of the central limit theorem, concerning the distribution of the average  $S_N$  of  $N$  random numbers  $S_N = 1/N \sum x_i$ . The macroscopic toughness limit,  $K^*$ , would play the role as  $\langle x \rangle$ , the variance of  $S_N$

decreases as a power-law of  $N$ , as the variance of the toughness does with the crack length, and the rescaled distribution of  $(S_N - \langle S_N \rangle) / \sqrt{\langle S_N^2 \rangle - \langle S_N \rangle^2}$  follows a universal (here Gaussian) distribution comparable to  $\psi$  in the sense of its independence with respect to the distribution of  $x_i$  or local toughness. In the following, this scaling property is exploited in the indentation geometry to develop a unified analysis of crack arrest statistics.

### 3 Application to indentation crack arrest

A very simple approach to crack arrest statistics is developed within a one-dimensional picture. Assuming a crack propagating across a layered material, the crack length statistics is written as [Chudnovsky and Kunin, 1987; Jeulin, 1994; Charles and Hild, 2002; Charles et al., 2003]

$$Q(c) = \prod_{i=1}^{c/\xi} F[K(i\xi)] \approx \exp\left(\frac{1}{\xi} \int_0^c \log F[K(x)] dx\right) \quad (7)$$

where  $Q(c)$  is the probability of having a crack length greater than  $c$ ,  $F[K_c]$  the probability that the toughness be less than  $K_c$ ,  $K(x)$  the value of the SIF at location  $x$  and  $\xi$  is the width of one layer or the correlation length in case of a random continuous toughness field. This result simply relies on the statistical independence of the toughness value between successive layers. It also allows one to account for the dependence of the SIF on the crack length. However, as such, it is dependent on the material properties through the entire function  $F$ , and the interpretation of the length scale  $\xi$  although clear for a layered system remains to be clarified for more heterogeneous systems.

Let us now address the question of crack arrest in a Vickers indentation experiment, considering a radial crack system. From the above section, some fundamental results are at hand to reduce significantly the specificity of the problem applied to a given material. One particularity of the problem is that the (radial) crack is semi-circular of radius  $c$  and hence the crack length  $L$  is proportional to its propagation distance  $c$ . In the modeling of the problem as one-dimensional (*i.e.*, simply parameterized by  $c$ ), to avoid correlations in the global critical SIF one has to resort to a coarse-grained discrete description. The crack front is correlated over its entire length  $L = \pi c$  and over a width  $w \propto \sigma_0 \xi^{1-\zeta} L^\zeta$  where  $\sigma_0 = \Sigma_0 / K^*$  corresponds to the standard deviation of the relative toughness fluctuations at the microscopic scale  $\xi$ . In the indentation geometry, the crack is thus regarded as propagating through a series of discrete shells whose width depends on the radius as  $w \propto c^\zeta$ . Moreover, each of these shells, will have a different statistical distribution of toughness (same  $K^*$  but different width  $c^{-1/\nu}$ ). Yet, these unexpected features are taken into account rigorously, and one arrives (see [Charles et al., 2004] for details) at the full expression of the crack length probability distribution.

Let us first introduce  $c^*$ , the crack radius which would occur if the toughness were homogeneous at its thermodynamic asymptotic value  $K^*$ , *i.e.*,  $K(c^*) = K^*$ . As mentioned earlier, in the present case of indentation, the toughness disorder induces a systematic  $R$ -curve effect. The larger the applied mass, the larger the apparent toughness (although the upper bound does not change with the crack size, whereas the mean value does). For a given applied mass, the value  $c^*$  is a lower bound on the crack size at arrest. For a large crack size as compared to the scale of heterogeneities, the propagation probability is written as

$$Q(c) \approx \exp \left\{ -A_0 \sigma_0^{\frac{\zeta-2}{1-\zeta}} \left( \frac{c^*}{\xi} \right)^{2-\zeta} \times \int_{c^*}^c \left( \frac{r}{c^*} \right)^{1-\zeta} \left( \frac{K^* - K(r)}{K^*} \right)^{\frac{1}{1-\zeta}} \frac{dr}{c^*} \right\} \quad (8)$$

where again  $A_0$  is a constant of the order of unity.

Let us further assume that the SIF follows a power law decrease with the crack radius  $K(c) \propto F/c^m$ , where asymptotically (for large loads)  $m = 3/2$ . In fact, one may argue that this essentially elastic-brittle description ( $m = 3/2$ ) has to be corrected by a dimensionless function of the ratio  $c/a$  to account for plasticity effects for  $c/a < 2$ . Lacking a safe experimental background for justifying such a systematic effect, an effective general power law dependence is introduced, and reverts to the value  $m = 3/2$  for large loads or as a first estimate for  $m$

$$Q(c) \approx \exp \left\{ -A_0 \sigma_0^{\frac{\zeta-2}{1-\zeta}} \left( \frac{c^*}{\xi} \right)^{2-\zeta} \times \int_1^x u^{1-\zeta} (1 - u^{-m})^{1/(1-\zeta)} du \right\} \quad (9)$$

with  $x = c/c^*$ . The integral in Eq. (9) is recast in a more compact form

$$Q(c) = \exp \left[ -A_0 \left( \frac{c^*/\xi}{\sigma_0^{1/(1-\zeta)}} \right)^{2-\zeta} \mathcal{B} \left( \frac{\zeta-2}{m}, \frac{2-\zeta}{1-\zeta}, \left( \frac{c}{c^*} \right)^{-m} \right) \right] \quad (10)$$

where  $\mathcal{B}$  is based on an incomplete beta function

$$\mathcal{B}(\mu, \eta, x) = \frac{\mu(1-\eta)}{\eta} \int_x^1 \tau^{\mu-1} (1-\tau)^{\eta-1} d\tau \quad (11)$$

The width of the distribution thus only depends i) on the system size  $c^*/\xi$  and ii) on the strength  $\sigma_0$  of the relative toughness disorder at the microscopic scale.

It may be noted that the same type of distribution was chosen *a priori* by Charles and Hild [2002]. Equation (9) therefore constitutes an *a posteriori* validation, even though the “grain size” is no longer constant in the present analysis. Let us also recall that  $2 - \zeta \approx 1.61$  [Rosso and Krauth, 2002; Vandembroucq and Roux, 2004].

#### 4 Experimental material and methods

The previous analytical results are now tested against experimental data. Several indentation tests, with different applied masses  $M$  (*i.e.*,  $F \propto M$ ), have been performed ( $M = 0.2$  kg,  $0.3$  kg,  $0.5$  kg and  $1$  kg) on four different brittle materials, namely alumina ( $\text{Al}_2\text{O}_3$ ), silicon nitride ( $\text{Si}_3\text{N}_4$ ), silicon carbide (SiC) and sodalime silicate glass. The microstructure of alumina is made of fine-grain (*i.e.*,  $10\mu\text{m}$ ) alumina polycrystals with an inter-granular glassy phase. A microanalysis shows that the latter contains  $\text{SiO}_2$ , CaO and  $\text{Al}_2\text{O}_3$  components. Silicon nitride is isostatically pressed with an average grain size close to  $3\mu\text{m}$ . The silicon carbide material is sintered. The powder was pressed and heated to  $2000$  degrees Celsius. During this step, small quantities of boron carbide have been added to improve the sintering process. A small porosity is induced by this manufacturing process. The SiC microstructure consists of grains whose characteristic length is estimated to  $4\mu\text{m}$ . Last, the studied glass is a standard float grade, of typical composition  $72$  wt%  $\text{SiO}_2$ ,  $14$  wt%  $\text{Na}_2\text{O}$ ,  $9.5$  wt% CaO,  $4.5$  wt% MgO, with traces of  $\text{K}_2\text{O}$ ,  $\text{Fe}_2\text{O}_3$ , and  $\text{Al}_2\text{O}_3$ . Beyond the nanometer scale glass is regarded as homogeneous.

After each indentation test, the length  $c$  of the cracks and the diagonal  $2a$  of the plastic print are measured. For the chosen loading range, it was checked that the radial-median crack system is predominant, following a  $c/a$  criterion [Ponton and Rawlings, 1989a,b]. In the case of alumina, additional observations have been performed to check that indentation-generated cracks (for an applied mass of  $1$  kg) remained connected to the plastic mark after polishing, thus discriminating the radial-median crack system from a Palmqvist one. Consequently only indentation results related to a ratio  $c/2a$  greater than  $1$  are used with the only exception of results obtained on  $\text{Si}_3\text{N}_4$  for which all crack lengths are such that  $c/2a < 1$ . In the latter case, the Palmqvist crack system is likely to be predominant. The questions of the identification and the effect of the crack system on the statistical analysis presented in this paper are discussed in Section 6.1 in more details. For each series of tests performed with the same load, the measured crack lengths  $c_i$  are associated to an experimental propagation probability  $Q(c_i)$ . The crack lengths are ranked in ascending order (*i.e.*,  $c_1 < c_2 < \dots < c_N$ ) and the corresponding experimental probability is evaluated as  $Q(c_i) = 1 - i/(N + 1)$ , where  $N$  is the number of measured crack radii for the considered applied mass.

Before any indentation test, the given material sample has been polished. This allows one to present an almost perfectly planar surface below the indenter and to better control the perpendicularity of the surface with respect to the indentation axis. Furthermore, this additional polishing process substantially decreases possible surface residual stresses which would affect the crack propagation conditions, and introduce some bias in the crack length measurements.

Beyond uncertainties due to the sample preparation, the measured indentation-generated crack length is strongly dependent on both the observation equipment and the experimentalist. To account for these parameters, one may compare data obtained with two different indentors on the same material and under the same conditions. It appears that the measured crack length strongly depends on the optical observation, but its influence on the measured crack length *scatter* is rather low. Last, one compares results obtained by two different operators measuring the same crack length, in order to evaluate its influence in the definition of the crack tip location. Again, although the measured absolute crack length may be operator-dependent, the scatter remains comparable.

## 5 Identification results

In the following analysis, data obtained on a sodalime silicate glass are analyzed to discuss different identification strategies. Equation (9) is simply rewritten as

$$Q(c) = \exp \left[ -A (c^*)^{2-\zeta} \mathcal{B} \left( \frac{\zeta-2}{m}, \frac{2-\zeta}{1-\zeta}, \left( \frac{c}{c^*} \right)^{-m} \right) \right] \quad (12)$$

where

$$A = A_0 \left( \xi \sigma_0^{1/1-\zeta} \right)^{\zeta-2} \quad (13)$$

Only two parameters are to be identified, namely the scale parameter  $A$  and the characteristic radius  $c^*$  provided the value for  $m$  is known. A least squares technique is used to determine the unknown parameters by minimizing the difference between the measured and modeled propagation probabilities. Furthermore, a rescaling procedure is followed to collapse all the experimental data onto a *single* master curve. The rescaled propagation probability  $\tilde{Q}$  is defined as

$$\tilde{Q} = Q^q \quad (14)$$

and the dimensionless crack radius  $\tilde{c}$

$$\tilde{c} = \frac{c}{c^*} \quad (15)$$

where  $q$  will depend on the type of identification procedure. Different strategies are followed to analyze the experimental data.

### 5.1 Step 1: Test of the distribution shape

The first test concerns the ability of the proposed scaling form to account for the shape of the arrest length distribution, for each individual material and load level *treated independently*. For this purpose, the  $m$  exponent is set to its asymptotic value  $m = 3/2$ . Figure 2 shows experimental data obtained for sodalime silicate glass with the four different masses and the corresponding

identification for each load. A good agreement is obtained in terms of overall distribution, thereby validating the general form of the distribution given in Eq. (9). Both parameters depend upon the applied mass as shown in Fig. 3. Figure 4 shows the result of the rescaling procedure. In this approach, the power  $q$  is defined as

$$q = \frac{B_0}{A(c^*)^{2-\zeta}} \quad (16)$$

in which  $B_0$  is chosen as the geometric average of the products  $A(c^*)^{2-\zeta}$  for all the applied masses. It is noted that out of 458 measurement points, only 18 are such that  $c/c^* < 1$  (none is expected theoretically).

### 5.2 Step 2: Test of the objectivity of material parameters

In the next identification stage, it is assumed that the parameter  $A$  is load-independent, as expected from Eq. (9), and characteristic of the material. Thus a further check of the prediction is that a single value for all load levels should account for all distributions. The constancy of  $A$  is thus prescribed during the identification stage. In contrast, the radius  $c^*$  is still assumed to be load-dependent. It is to be noted that  $c^*$  is the result of an intrinsic material parameter  $K^*$ , together with a relationship between  $K$ ,  $F$  and the crack radius modeled by a power law of exponent  $m$ . As one dealt experimentally with rather short cracks, the latter relation may deviate from the simple power law dependence,  $m = 3/2$ . Thus at this stage,  $m$  is still set to its asymptotic value, but  $c^*$  is considered as a free parameter determined for each load.

Figure 5 shows the result of the identification. A good agreement is obtained, even though not as good as in the previous case (as naturally expected because the functional form is more constrained). The value of  $A^{1/(2-\zeta)}$  is found to be equal to  $0.57 \mu\text{m}^{-1}$ . Let us recall that this value is not directly read as an (inverse) characteristic correlation length that would signal the physical size of heterogeneities. The amplitude of the microscopic toughness distribution,  $\sigma_0$  does contribute to  $A$ . Figure 6 shows the dependence of the characteristic radius  $c^*$  with the applied mass  $M$ . The observed dependence is close to what is expected from the model [*i.e.*,  $c^* \propto M^{2/3}$  through the definition of a stress intensity factor  $K^* \propto M/(c^*)^{3/2}$ ]. Since the parameter  $A$  is constant, the power  $q$  of the rescaled propagation probability is now given by

$$q = \left(\frac{c_0}{c^*}\right)^{2-\zeta} \quad (17)$$

in which  $c_0$  is chosen as the geometric average of the characteristic radii  $c^*$  for all the applied masses. Figure 7 shows the prediction for the indentation experiments on glass. Only nine points are such that  $c/c^* < 1$ .

### 5.3 Step 3: Complete test of the prediction

The final test would consist in enforcing the  $K(c)$  dependence with  $m = 3/2$  in the identification procedure. It leads to a significant degradation of the quality of the results. As mentioned earlier, in most of the test cases, the ratio of the crack length to the half diagonal of the plastic imprint is too small to trust the asymptotic  $K(c)$  law. As observed in the previous step, Fig. 6,  $c^*$  deviates from the expected power law of exponent  $1/m = 2/3$ . Such deviations are not surprising when dealing with small values of the ratio  $c/a$ , plasticity being thus the main dissipation mechanism.

However, one also notes that an *effective* power law fits the data quite nicely. Let us insist on the fact that this is a purely empirical observation, which is not supported by any theoretical argument, nor by the literature that proposes numerous conflicting laws [Ponton and Rawlings, 1989a]. If one introduces  $m'$  the exponent such that

$$c^* \propto M^{1/m'} \quad (18)$$

one measures  $1/m' \approx 0.8$  for glass (Fig. 6). Note that the scaling  $K \propto M/c^{3/2}$  is only expected to hold for  $c/a > 2$ ;  $c/a$  dependent corrections to scaling being necessary when  $c/2a$  is closer to unity. The value of the effective exponent  $1/m'$  is thus expected to approach  $2/3$  as the ratio  $c/a$  increases. See also Subsection 6.1 for a detailed discussion about the dependence of  $m$  on the nature of the crack system.

Such an observation is however unsatisfactory in the sense that a power law dependence involving  $m$  has already been used in the derivation of the functional forms which allowed one to estimate  $m'$ . Thus, as a final self-consistency requirement, it is proposed to determine the best parameter  $m$  such that the observed  $m'$  matches its starting value  $m$ . This self-consistent  $m$  value is determined numerically using a fixed point algorithm, *i.e.*, setting  $m$  to a previously determined  $m'$  until convergence. In one iteration the value of the power is unaltered for three representative digits. Furthermore, the predictions are very close to those obtained in Figs. 5 and 7 since the initial value  $m'$  is already very close (*i.e.*, 99 %) to its converged estimate.

### 5.4 Application to four different brittle materials

The results obtained for the four different brittle materials ( $\text{Al}_2\text{O}_3$ , SiC,  $\text{Si}_3\text{N}_4$ , glass) are presented when using the above described statistical treatments.

**5.4.1 Step 1** By following the first identification stage, one obtains the following results:

- for alumina, when one operator and one indentation machine is used (Fig. 8-top) and two operators and two different machines (Fig. 8-bottom). A very good agreement is obtained in both cases and no significant deviation is observed when two operators and two indentors are used when compared to a single set of measurements.
- for silicon nitride when one operator and one indentation machine is used (Fig. 9). Note here that despite the fact that the crack lengths are characterized by a low  $c/a$  ratio, the experimental results are very well described by the analytical expression (9) obtained while setting  $m$  to  $3/2$  only valid *a priori* for  $c/a > 2$ .
- for silicon carbide when one operator and one indentation machine is used (Fig. 10-top) and two operators and two different machines (Fig. 10-bottom). It is noted that the two sets of results are again very close.
- for glass when one operator and one indentation machine is used (Fig. 11-top) and two operators and two different machines (Fig. 11-bottom). It is noted that the two sets of results are also very close.

This first identification stage gives very good results. For all materials, the crack length distributions obtained for various loads collapse onto a single master curve. Comparing Figs. 8, 9, 10, 11 one observes that the width of the distributions varies noticeably from material to material. The median crack length  $c_m/c^*$  such that  $Q(c_m) = 0.5$  is measured to be  $c_m/c^* \approx 1.7$  for  $\text{Al}_2\text{O}_3$ , 1.35 for  $\text{Si}_3\text{N}_4$ , 1.5 for  $\text{SiC}$  and 1.15 – 1.2 for glass. As discussed above, the width of the crack length distribution depends upon two parameters. It first decreases with the system size ( $c^*/\xi$ ) so that the finer the microstructure (or the smaller the toughness) the narrower the distribution. Second, it depends on the width of the toughness disorder at the microscopic scale. The stronger the toughness disorder, the larger the distribution. In the present case, not surprisingly, glass which is characterized by a low toughness and a very small correlation length for the disorder gives the narrowest distribution. Conversely the largest distribution is obtained for the alumina ceramic which has the coarser microstructure and the highest toughness of the tested materials (except silicon nitride).

*5.4.2 Step 2* By using the second identification stage, one obtains the following results:

- for alumina (Fig. 12) the uncertainty on  $c^*$  is  $3 \mu\text{m}$  when the same machine is used, and less than  $4 \mu\text{m}$  when the two different machines are utilized.
- for silicon nitride when one operator and one indentation machine is used (Fig. 13), an uncertainty less than  $3 \mu\text{m}$  on  $c^*$  is found.
- for silicon carbide when one operator and one indentation machine is used (Fig. 14-top), and two different machines with two operators (Fig. 14-bottom). When the same parameter  $A$  is considered for the three different experimental conditions, an uncertainty less than  $3 \mu\text{m}$  on  $c^*$  is found when the same machine is used, and less than  $5 \mu\text{m}$

when two different machines are utilized. The first load level is not well described. Again this is explained by the fact that, the ratios  $c/a$  being in this case very close to 2, a competition is observed between the Palmqvist and the radial/median crack systems. It is thus likely that even if the dependence between  $c^*$  and  $M$  is approached by an adapted power law relationship, the data corresponding to the two crack systems cannot be treated together.

- for glass when one operator and one indentation machine is used (Fig. 15-top), and two operators and two different machines (Fig. 15-bottom). When the same parameter  $A$  is considered for the two different experimental conditions, an uncertainty less than  $7 \mu\text{m}$  on  $c^*$  is found.

*5.4.3 Step 3* The self-consistency was checked for all the situations. Figure 16 shows the dependence of the characteristic radius  $c^*$  with the applied mass  $M$ . When a power law dependence is sought, all conditions apart from silicon nitride have approximately the same exponent (*i.e.*,  $1/m' \approx 0.8$  compared to the expected asymptotic value 0.67). When the fixed-point algorithm is used, the difference between the first estimate of  $m'$  and its converged value is always less than 4% for all the analyzed cases. Furthermore, convergence is very fast since at most three iterations were used to get the final results.

## 6 Discussion

The present analysis was obtained using two main hypotheses, namely, an elastic-brittle behavior and strong pinning conditions. Moreover the crack system was assumed to be radial/median. In the following, the results of the statistical analysis are discussed in the light of these different hypotheses.

### 6.1 nature of the crack system

Table 1 summarizes the results obtained for the effective exponent  $m$  and the ratio  $c/a$  for the various materials and experimental conditions. The same results are presented in Fig. 17. Looking at the dependence of the measured exponent  $1/m'$  on the average  $c/2a$  value, one clearly distinguishes two groups of materials. The first one consists of silicon nitride and the other one of glass and silicon carbide. As described above average crack length values for silicon nitride are less than the other ones. Moreover exponent values are also lower and close to 0.5-0.6. Conversely, SiC (1), SiC (3), glass (1) and glass (3) exponents all concentrate close to 0.8, and seem to approach closer to this value when the ratio  $\langle c/2a \rangle$  increases (even if this change is not monotonic). The case of alumina is more dubious, even the results corresponding to large  $c/a$  values do not exhibit a clear belonging to any of these two groups.

These separate behaviors are attributed to the nature of the crack system. As discussed above, the present study is developed in the framework of a median/radial crack system. However, the Palmqvist crack system classically appears for high toughness materials. In the case of low toughness materials, the crack system is predominantly median/radial for high loads but may be of Palmqvist type if the applied load is low enough. Experimentally, it is difficult to discriminate between these two crack systems without direct observation. In particular, the value of the ratio  $c/2a$  is often not sufficient to predict the generated indentation-crack [Glandus and Rouxel, 1991]. Beyond the influence on the ratio  $c/a$ , the nature of the crack system also affects the scaling of the crack length with load, namely, a Palmqvist crack system generates the scaling  $l \propto M$  (with  $l = c - a$ ), while a radial one induces  $c \propto M^{2/3}$ . For silicon nitride,  $c/2a$  values obtained during indentation experiments, and the unusual values for  $1/m'$ , allow us to conclude that the generated crack system is of Palmqvist type, namely, for such a material, Wang et al. [2002] have reported a change in the crack system for  $c/a$  between 2.3 and 2.4.

The dependence of the scaling behavior on the nature of the crack system is seen again when plotting the exponent  $m$  against the applied mass (Fig. 18). One observes first that the two above identified groups still exist, namely, silicon nitride exponents exhibit a (decreasing) convergence toward 0.4-0.45 when the applied mass increases, while both glass and silicon carbide exponents converge toward 0.8. The previous conclusions on the generated crack system for these materials are therefore confirmed.

Let us now discuss the behavior of alumina exponents. Namely, when the applied mass increases, so does  $1/m'$  from silicon nitride exponent values to glass and silicon carbide ones. One concludes that for high applied loads, the indentation generated crack system is the same as for glass (or silicon carbide). Yet, for low applied loads, this system is closer to a Palmqvist or a mixed system. To conclude on the latter crack systems as a function of the applied mass, one would have to perform additional experiments with both lower and higher load levels, and direct observation of the developed cracks should be carried out.

By considering the results obtained for silicon carbide, glass, and partially for alumina, one concludes that the identified values for the exponent between  $c^*$  and the applied mass  $M$  are consistent with both theory and observations, even if one has to account for an “asymptotic”  $1/m'$  value for radial crack systems greater than the expected one (0.8 instead of 0.67). The universal distribution proposed to describe the statistics of indentation crack lengths gives a satisfactory account of most of the experimental data obtained on different materials. Moreover the few experimental data not properly described by this approach developed in the framework of a median/radial crack system may be attributed to Palmqvist indentation cracks.

## 6.2 Microscopic interpretation

As discussed above, the statistical analysis allows us to extract a microscopic parameter  $A$  that is re-expressed as a typical length, namely,  $A^{1/\zeta-2} = A_0^{1/\zeta-2} \xi \sigma_0^{1/1-\zeta}$ . This expression includes the characteristic size  $\xi$  of the heterogeneities as well as a factor dependent on the level of the local disorder. Table 2 summarizes the results obtained for the different materials studied herein. Let us compare them with estimated characteristic scales of the structural disorder. Apart from the case of glass, these results are consistent with relative toughness fluctuations of order 1. Note however that these results have to be considered cautiously. Two hypotheses of the analysis may affect the interpretation of the parameter  $A$  and more specifically the length scale  $\xi$ . The assumption of an elastic-brittle behavior imposes one to consider crack fronts of extension greater than the size of the process zone. The latter is thus a lower bound for  $\xi$  even if a structural disorder may exist at finer scales. A more questionable point is the hypothesis of strong pinning. The latter corresponds to situations where the structural disorder is strong enough to locally arrest the crack front. As discussed above, this induces an intermittent dynamics of the crack propagation. Conversely, in weak pinning conditions, the toughness disorder only modulates the front conformation and crack fronts change smoothly. It is shown that strong pinning conditions are always obtained in the limit of large fracture fronts [Roux et al., 2003]. In the case of a rather weak structural disorder, one thus may expect that the characteristic length  $\xi$  no longer be defined by the characteristic size of the heterogeneities but by a larger scale corresponding to the transition between weak and strong pinning.

## 7 Summary

By using a model developed to characterize the statistical properties of a crack front propagating through a heterogeneous material, an analytical expression is given for the distribution of crack arrest lengths. The latter was shown to be material-independent. The distribution presents a universal shape and is fully characterized by two parameters. The first one corresponds to the macroscopic toughness value. The second one, which gives the width of the distribution, depends on the relative size of the cracks compared the size of the microstructure and on the width of the microscopic toughness disorder (for very large sizes, the distribution tends to a Dirac centered on the macroscopic toughness value).

Experimental tests have been performed on four different materials (alumina, silicon nitride, silicon carbide and sodalime silicate glass) with four different loads (0.2 kg, 0.3 kg, 0.5 kg and 1 kg). A particular attention was given to potential sources of non-intrinsic fluctuations, namely the dependence on the operator and on the testing machine. It appeared that the analytical expression gives a very good account of the data. Coupled with

experimental observations the statistical analysis allowed us to discriminate between indentation cracks belonging to a median/radial and a Palmqvist crack system, respectively. Restricting ourselves to the former case within which the present analysis was developed, fitting parameters consistent with the scaling laws expected in the geometry of indentation tests were obtained.

A very strong feature of the results obtained in the present work is that the knowledge of the crack length (or effective toughness) distribution at a given scale gives an immediate access to the distributions corresponding to any other scale. In particular, this should help improving the quality of crack length or toughness estimates for large systems when using data obtained at microscopic or a much finer scale.

### Acknowledgements

The authors acknowledge useful discussions with Pr. Tanguy Rouxel and Dr. René Gy.

### References

- E. Bouchaud, Scaling properties of cracks, *J. Phys. Cond. Mat.* **9** (1997) 4319-4344.
- Y. Charles and F. Hild, Crack arrest in ceramic/steel assemblies, *Int. J. Fract.* **15** [3] (2002) 251-272.
- Y. Charles, F. Hild and S. Roux, Long-term reliability of ceramics: The issue of crack arrest, *ASME J. Eng. Mat. Tech.* **125** (2003) 333-340.
- Y. Charles, D. Vandembroucq, F. Hild and S. Roux, Material independent crack arrest statistics *J. Mech. Phys. Solids* **52** (2004) 1651-1669.
- A. Chudnovsky and B. Kunin, A probabilistic model of brittle crack formation, *J. Appl. Phys.* **62** (1987) 4124-4129.
- R.F. Cook, B.R. Lawn and C.J. Fairbanks, Microstructure-strength properties: I. Effect of crack size on toughness, *J. Am. Ceram. Soc.* **68** (1985) 604-615.
- H. Gao and J.R. Rice, A first order perturbation analysis on crack trapping by arrays of obstacles, *J. Appl. Mech.* **56** (1989) 828-836.
- J.C. Glandus and T. Rouxel, Study of the Y-TZP Toughness by an Indentation Method, *Ceram. Inter.* **17** (1991) 129-135.
- H.J. Herrmann and S. Roux, *Statistical models for the fracture of disordered media*, North-Holland (1990).
- A. de S. Jayatilaka and K. Trustrum, Statistical approach to brittle fracture, *J. Mater. Sci.* **12** (1977) 1426-1430.
- D. Jeulin, Fracture statistics models and crack propagation in random media, *Appl. Mech. Rev.* **47** [1] (1994) 141-150.
- J.-F. Joanny and P.G. de Gennes, A model for contact angle hysteresis, *J. Chem. Phys.* **81** (1984) 552-562.

- C.R. Kurkjian, *Strength of inorganic glass*, Plenum Press, New York (USA), (1985).
- B.R. Lawn, A.G. Evans and D.B. Marshall, Elastic/plastic indentation damage in ceramics: The median/radial crack system, *J. Am. Ceram. Soc.* **63** [9-10] (1980) 574-581.
- B. R. Lawn, *Fracture of brittle solids*, Cambridge University Press, Cambridge (UK), (1993).
- C. B. Ponton and R. D. Rawlings, Vickers indentation fracture toughness test - Part 1 - Review of literature and formulation of standardized indentation toughness equations, *Mat. Sci. Tech.* **5** (1989) 865-872.
- C. B. Ponton and R. D. Rawlings, Vickers indentation fracture toughness test - Part 2 - Application and evaluation of standardized indentation toughness equations, *Mat. Sci. Tech.* **5** (1989) 961-976.
- A. Rosso and W. Krauth, Roughness at the depinning threshold for a long-range elastic string, *Phys. Rev. E* **65** (2002) 025101.
- S. Roux, D. Vandembroucq and F. Hild, Effective toughness of heterogeneous brittle materials *Eur. J. Mech. A/Solids* **22** (2003) 743-749.
- J. Schmittbuhl, S. Roux, J.-P. Vilotte and K.J. Maloy, Interfacial crack pinning: effect of non-local interaction, *Phys. Rev. Lett.* **74** (1995), 1787-1790.
- J. Schmittbuhl and K. J. Måløy, Direct observation of a self-affine crack propagation, *Phys. Rev. Lett.* **78** (1997), 3888-3891.
- R. Skoe, D. Vandembroucq and S. Roux, Front propagation in random media: From extremal to activated dynamics *Int. J. Mod. Phys. C* **13** (2002) 751-757.
- D. Vandembroucq and S. Roux, Large scale simulations of ultrametric depinning, *Phys. Rev. E* **70** (2002) 026103.
- J. Wang, J. Gong and Z. Guan, Variation in the indentation toughness of silicon nitride, *Mat. Lett.* **57** (2002) 643-646.
- W. Weibull, *A statistical theory of the strength of materials*, Roy. Swed. Inst. Eng. Res., Report no. **151** (1939).

**Table 1** Identified exponent of the power law between  $c^*$  and the applied mass  $M$  and average normalized crack length for all studied materials and masses (expressed in kg), for (1) one operator and one indentation machine, and (3) two operators and two indentation machines

Mass (kg)	Parameters	Al <sub>2</sub> O <sub>3</sub>		Si <sub>3</sub> N <sub>4</sub>	SiC		Glass	
		(1)	(3)		(1)	(3)	(1)	(3)
1.0	$1/m'$	0.79	0.90	0.46	0.77	0.79	0.81	0.80
	$\langle c/2a \rangle$	1.41	1.24	0.76	1.51	1.37	1.72	1.66
0.5	$1/m'$	0.84	0.70	0.50	0.86	0.80	0.80	0.77
	$\langle c/2a \rangle$	1.13	1.15	0.77	1.30	1.28	1.47	1.41
0.3	$1/m'$	0.68	0.57	0.57	0.80	0.79	0.81	0.81
	$\langle c/2a \rangle$	1.27	1.13	0.77	1.24	1.24	1.28	1.28
0.2	$1/m'$	0.58	0.58	0.59	0.69	0.77	0.82	0.86
	$\langle c/2a \rangle$	1.31	1.41	0.76	1.178	1.178	1.17	1.17

**Table 2** Identified parameters  $A$  and estimation of the characteristic scales of the structural disorder for the four tested materials.

Mass (kg)	Parameters	Al <sub>2</sub> O <sub>3</sub>		Si <sub>3</sub> N <sub>4</sub>	SiC		Glass	
		(1)	(3)		(1)	(3)	(1)	(3)
-	$\xi$ ( $\mu\text{m}$ )	10		3	4		0.002	
1.0	$A^{\frac{1}{2-\zeta}}$ ( $\mu\text{m}^{-1}$ )	0.08	0.12	0.34	0.17	0.14	0.32	0.18
0.5		0.12	0.15	0.39	0.29	0.25	0.65	0.42
0.3		0.19	0.19	0.50	0.29	0.29	0.75	0.75
0.2		0.22	0.22	0.80	0.88	0.88	0.62	0.62

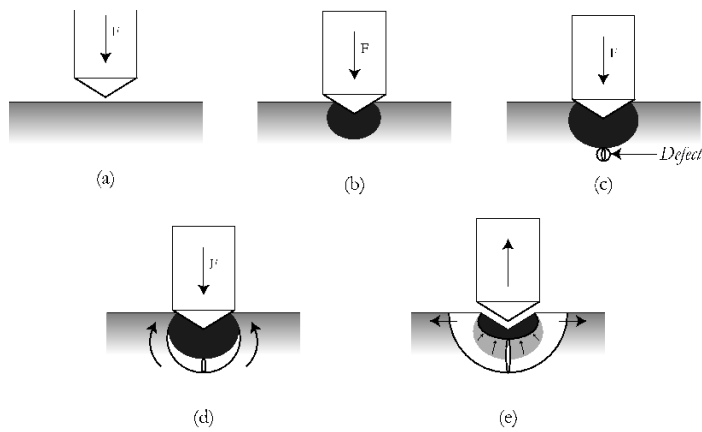


**Fig. 1** Indentation principle. At the beginning of the indentation test, a plastic zone is created below the Vickers pyramid (b), inducing residual stresses. When the total stress (*i.e.*, the applied one and the residual one) is large enough, two perpendicular elementary cracks are created at the deepest location under the plastic zone (c). For brittle media, it is admitted that cracks are initiated from material defects. These two cracks propagate along the plastic zone (d) when the load is about to reach its maximum value. Then, while unloading the sample, cracks finish their propagation, and their final form is semi-circular (e).

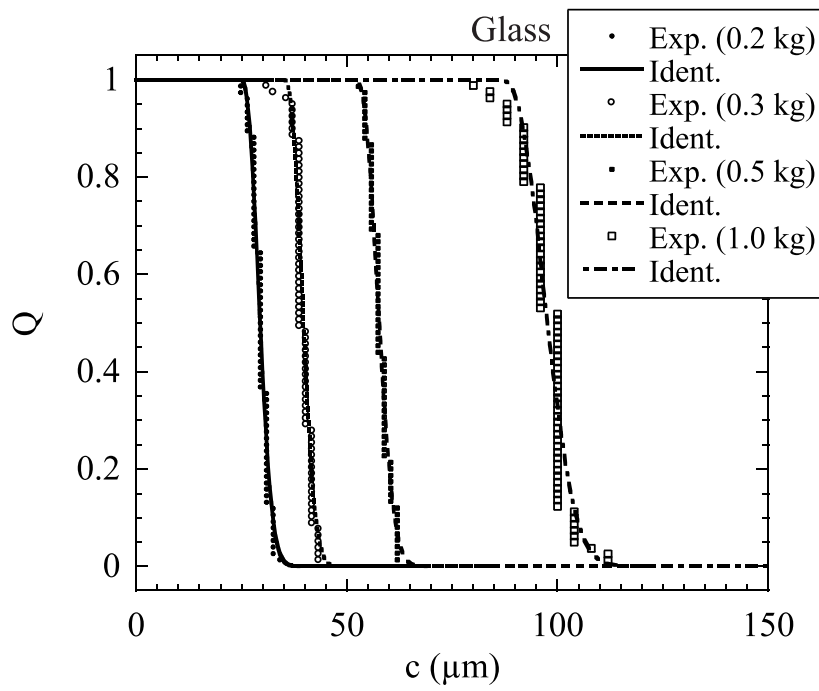


**Fig. 2** Propagation probability  $Q$  versus crack radius  $c$  for four different applied masses on soda-lime silicate glass. The symbols are experimental data and the lines are identifications when each load level is analyzed independently.

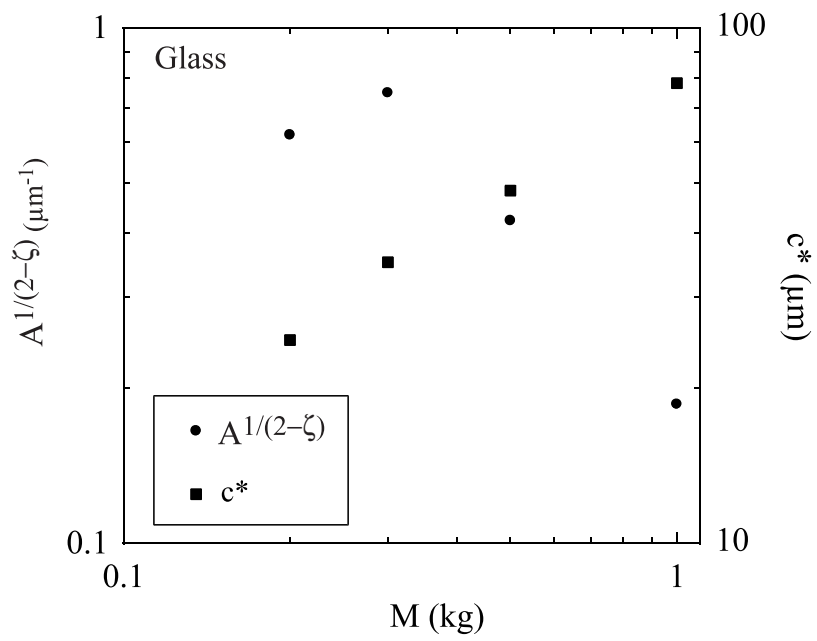


**Fig. 3** Parameters  $A$  and  $c^*$  versus applied mass  $M$  when each load level is analyzed independently for sodalime silicate glass.

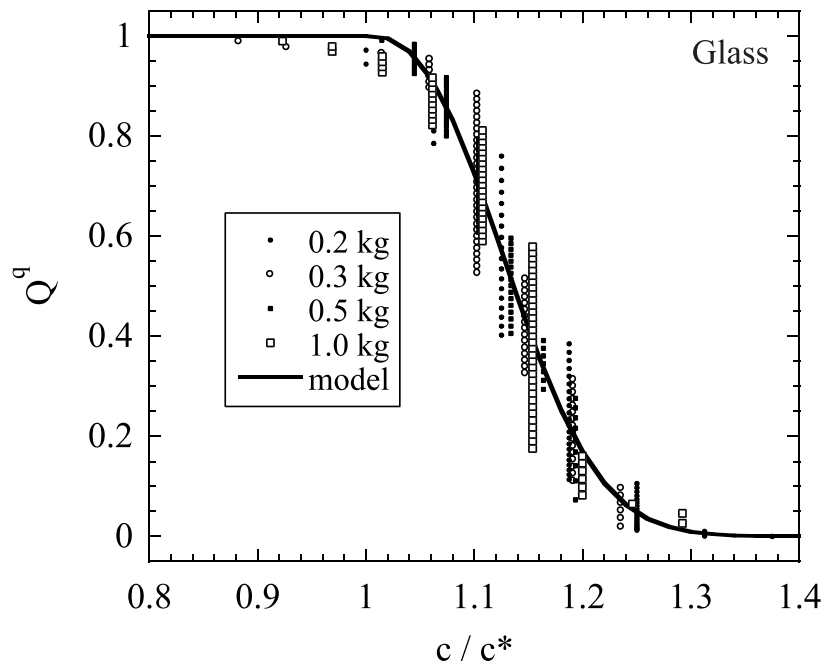


**Fig. 4** Rescaled propagation probability  $Q^g$  versus dimensionless crack radius  $c/c^*$  for four different applied masses. The symbols are experimental data of soda-lime silicate glass and the line is the result of the identification. From the present analysis, it is expected that all experimental points should fall on the same curve.

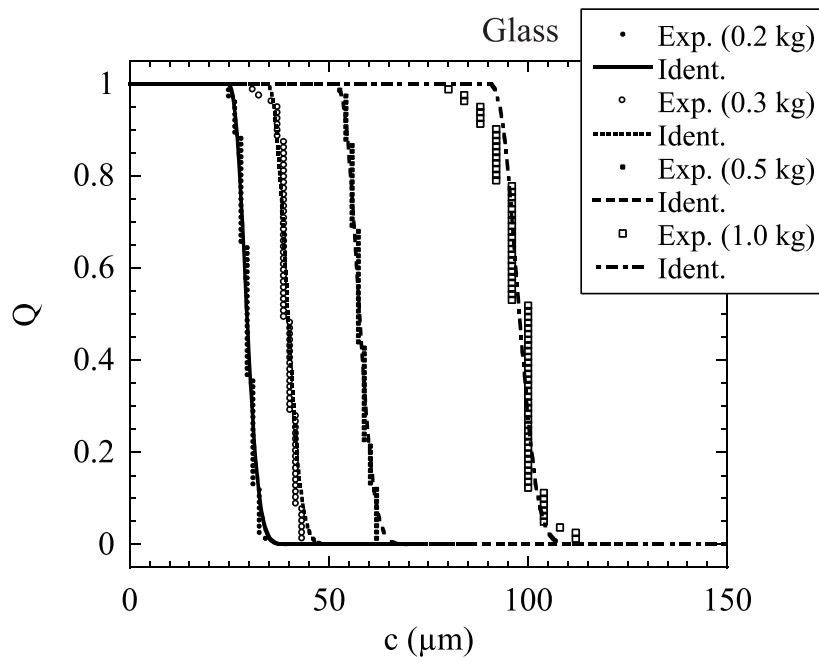


**Fig. 5** Propagation probability  $Q$  versus crack radius  $c$  for four different applied masses on sodalime silicate glass. The symbols are experimental data and the lines are identifications when the parameter  $A$  is assumed to be load-independent.

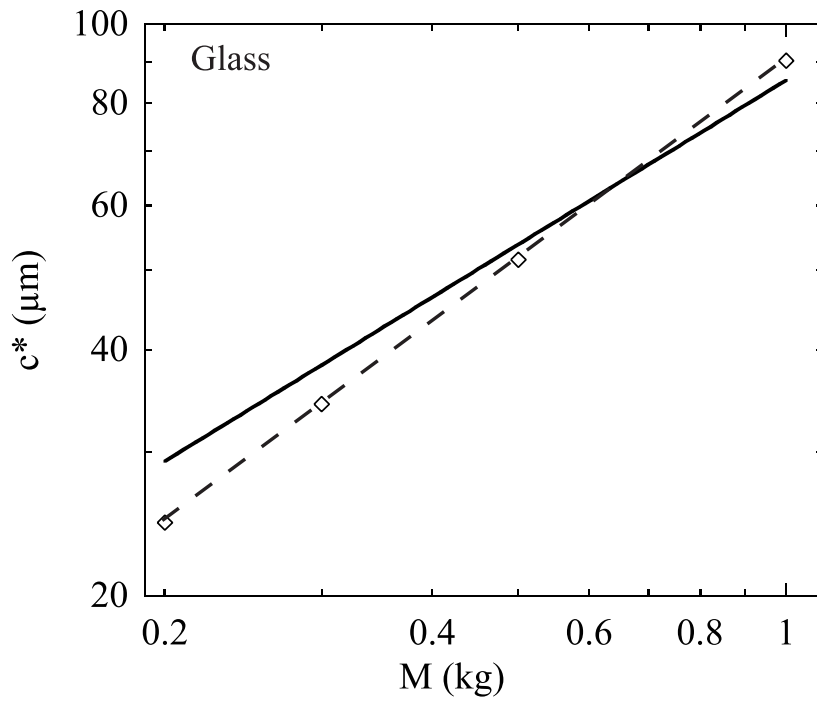


**Fig. 6** Parameter  $c^*$  versus applied mass  $M$ . A power law with an exponent of  $2/3$  fits reasonably the experiments on sodalime silicate glass (solid line). The dashed line corresponds to the best power law fit for an exponent equal to  $0.81$ .

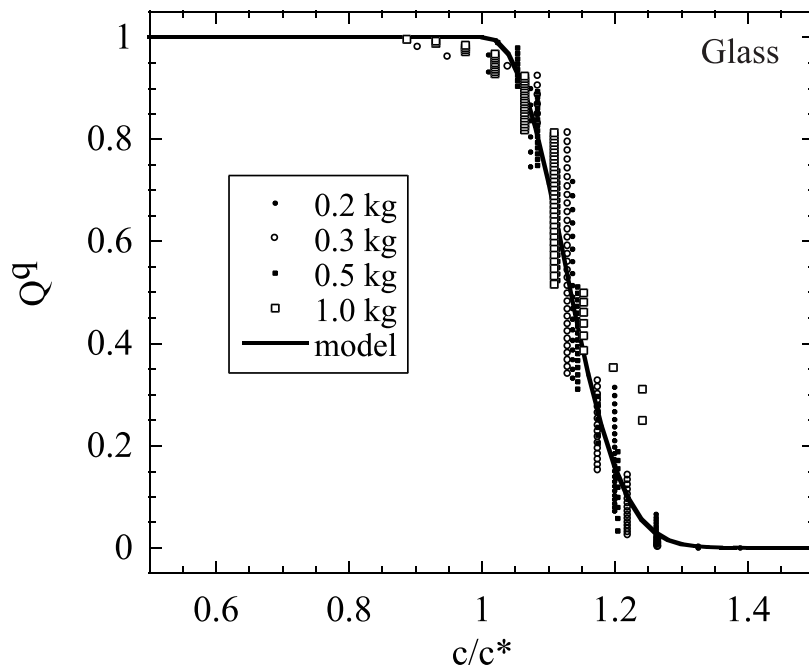


**Fig. 7** Rescaled propagation probability  $Q^g$  versus dimensionless crack radius  $c/c^*$  for four different applied masses. The symbols are experimental data on sodalime silicate glass and the line is the result of the identification with a constant parameter  $A$ . From the present analysis, it is expected that all experimental points should fall on the same curve.

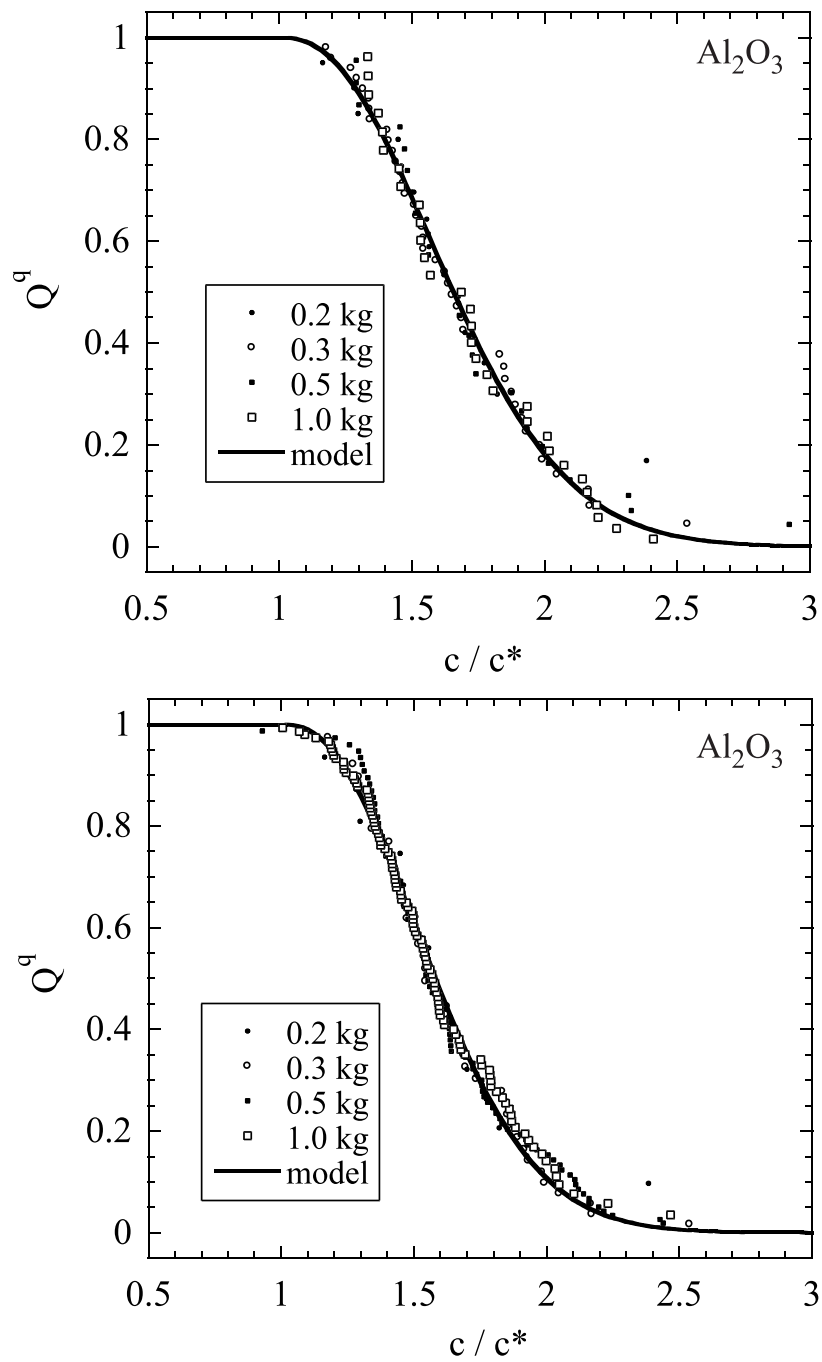


**Fig. 8** Rescaled propagation probability  $Q^q$  versus dimensionless crack radius  $c/c^*$  for four different applied masses on alumina. The symbols are experimental data and the line is the result of the identification. From the present analysis, it is expected that all experimental points should fall on the same curve. Top: 1 machine and 1 operator. Bottom: 2 indentors and 2 operators.

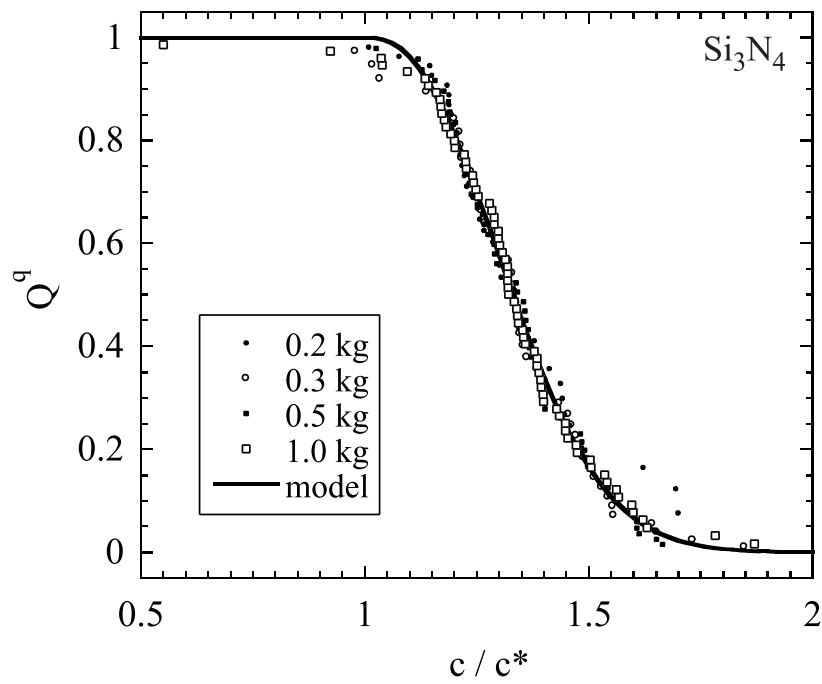


**Fig. 9** Rescaled propagation probability  $Q^q$  versus dimensionless crack radius  $c/c^*$  for four different applied masses on silicon nitride. The symbols are experimental data and the line is the result of the identification. From the present analysis, it is expected that all experimental points should fall onto the same curve.

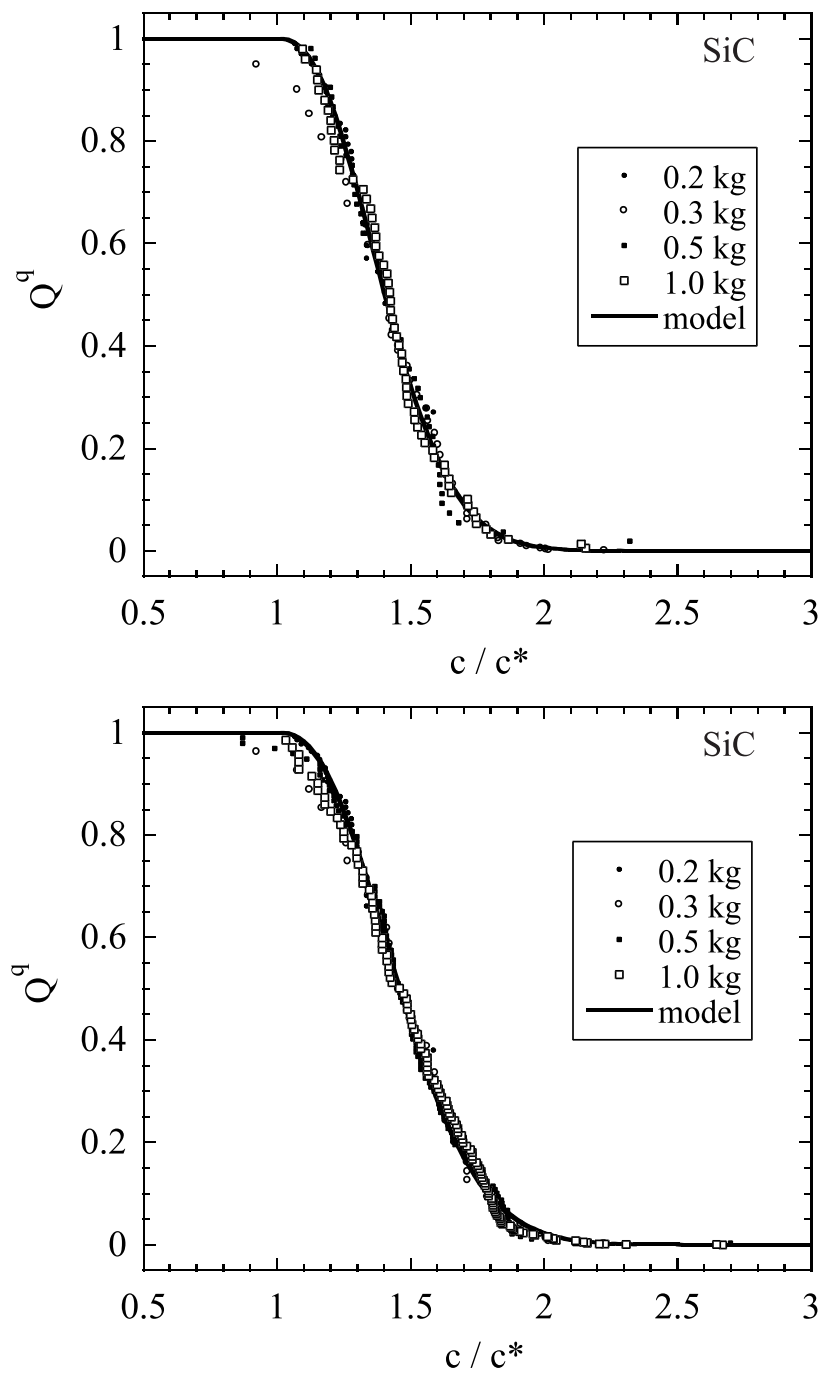


**Fig. 10** Rescaled propagation probability  $Q^q$  versus dimensionless crack radius  $c/c^*$  for four different applied masses on silicon carbide. The symbols are experimental data and the line is the result of the identification. From the present analysis, it is expected that all experimental points should fall on the same curve. Top: 1 machine and 1 operator. Bottom: 2 indentors and 2 operators.

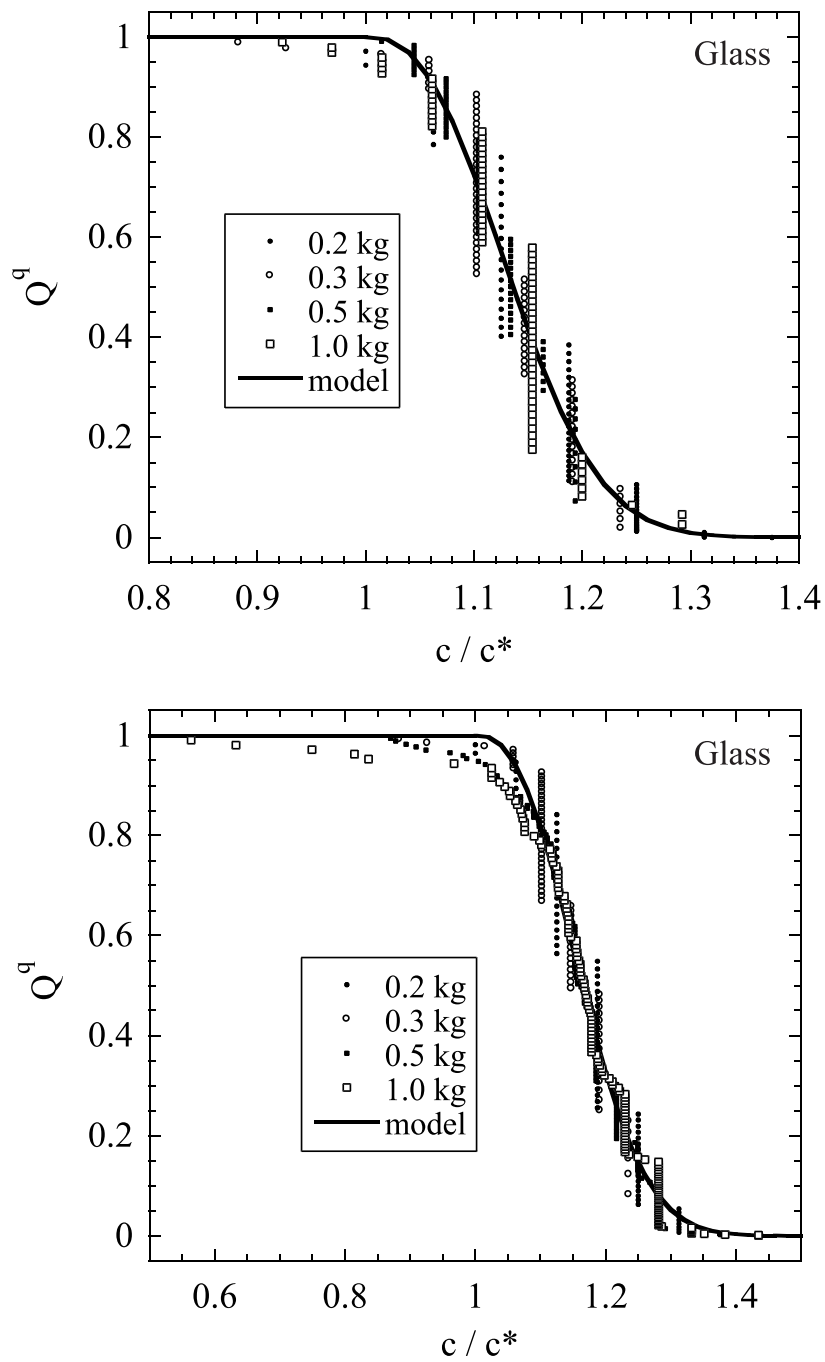


**Fig. 11** Rescaled propagation probability  $Q^q$  versus dimensionless crack radius  $c/c^*$  for four different applied masses on sodalime silicate glass. The symbols are experimental data and the line is the result of the identification. From the present analysis, it is expected that all experimental points should fall on the same curve. Top: 1 machine and 1 operator. Bottom: 2 indentors and 2 operators.

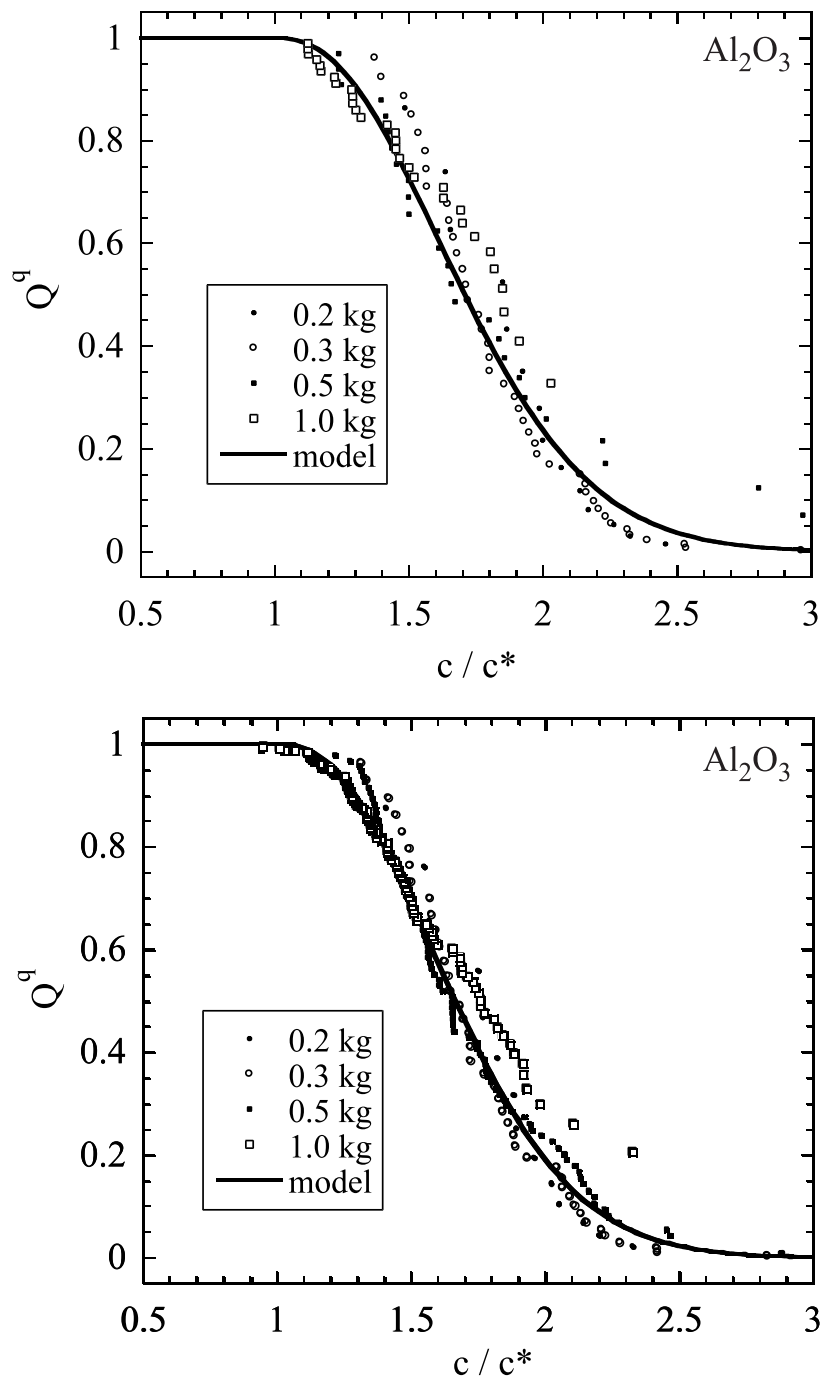


**Fig. 12** Rescaled propagation probability  $Q^q$  versus dimensionless crack radius  $c/c^*$  for four different applied masses on alumina. The symbols are experimental data and the line is the result of the identification with a constant parameter  $A$ . From the present analysis, it is expected that all experimental points should fall on the same curve. Top: 1 machine and 1 operator. Bottom: 2 indentors and 2 operators.

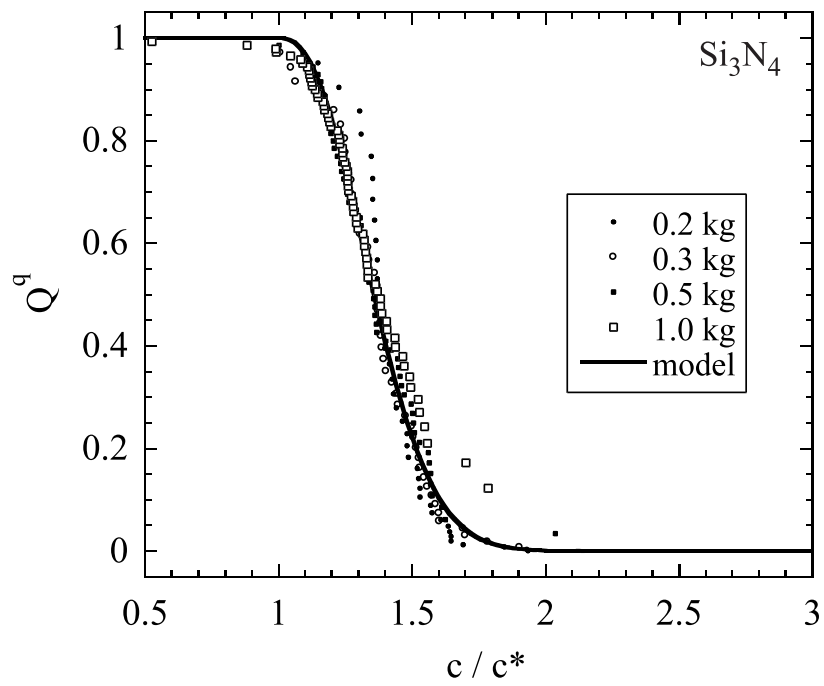


**Fig. 13** Rescaled propagation probability  $Q^p$  versus dimensionless crack radius  $c/c^*$  for four different applied masses on silicon nitride. The symbols are experimental data and the line is the result of the identification with a constant parameter  $A$ . From the present analysis, it is expected that all experimental points should fall on the same curve.

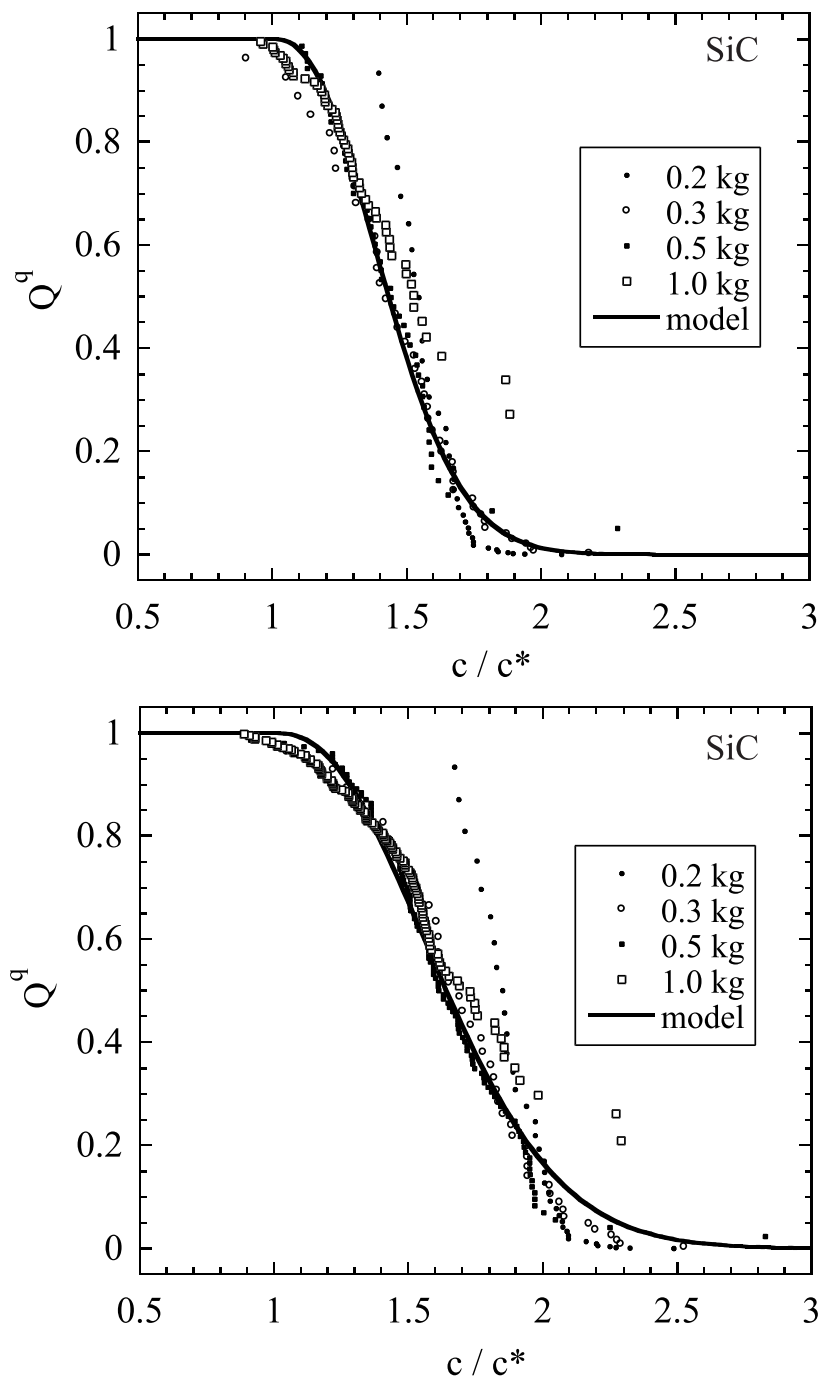


**Fig. 14** Rescaled propagation probability  $Q^q$  versus dimensionless crack radius  $c/c^*$  for four different applied masses on silicon carbide. The symbols are experimental data and the line is the result of the identification with a constant parameter  $A$ . From the present analysis, it is expected that all experimental points should fall on the same curve. Top: 1 machine and 1 operator. Bottom: 2 indentors and 2 operators.

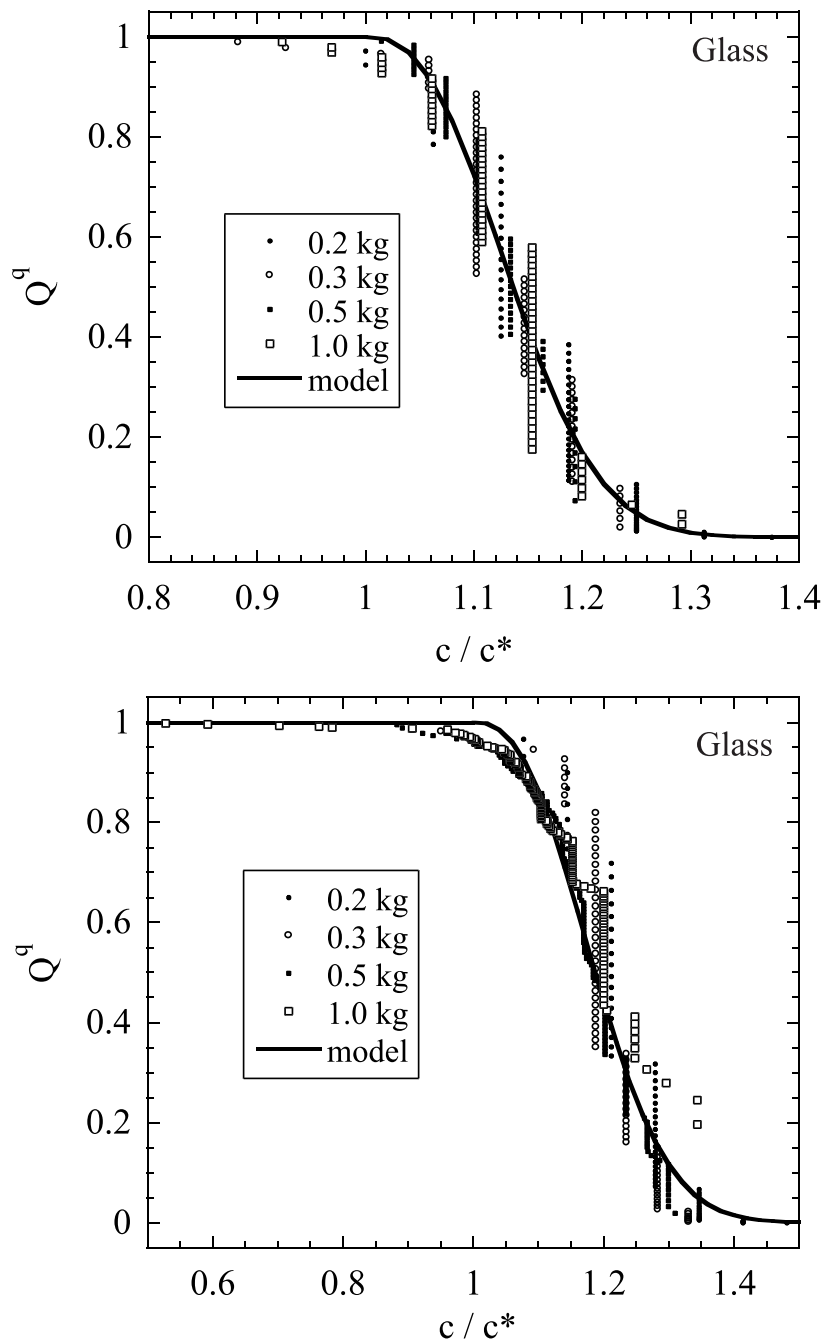


**Fig. 15** Rescaled propagation probability  $Q^q$  versus dimensionless crack radius  $c/c^*$  for four different applied masses on sodalime silicate glass. The symbols are experimental data and the line is the result of the identification with a constant parameter  $A$ . From the present analysis, it is expected that all experimental points should fall on the same curve. Top: 1 machine and 1 operator. Bottom: 2 indentors and 2 operators.

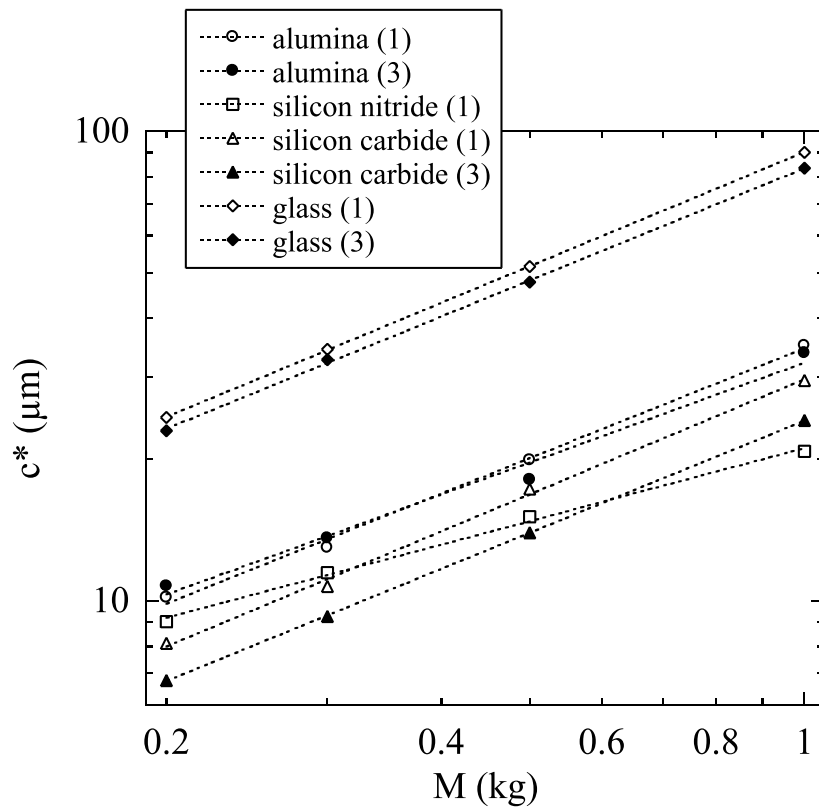


**Fig. 16** Parameter  $c^*$  versus applied mass  $M$  for the six series of experiments. A power law fits reasonably all the experiments (dashed lines). The number in parentheses indicates the number of situations (machine and operator) used to perform the identification

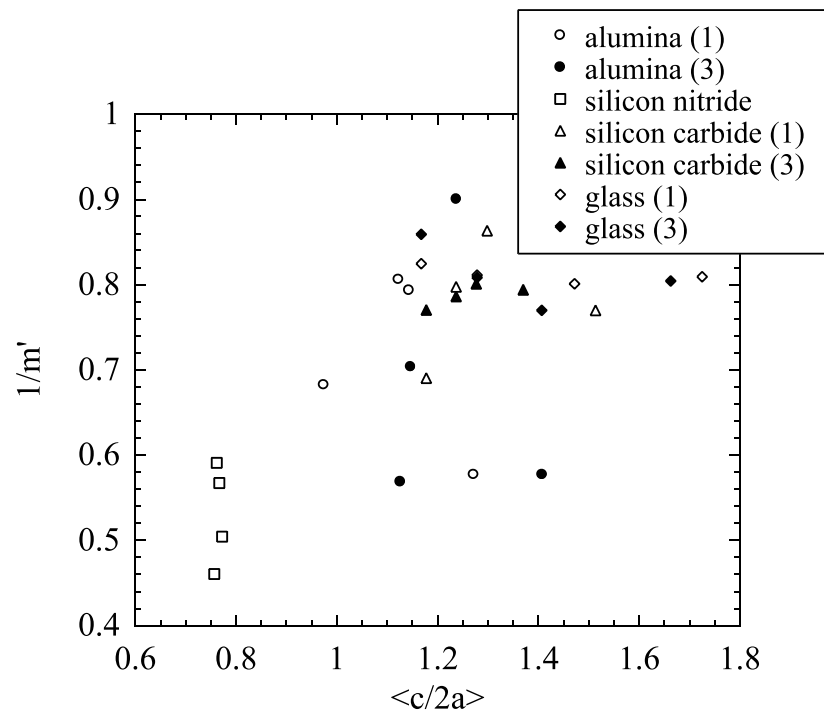


Fig. 17 Change of  $1/m'$  versus  $\langle c/2a \rangle$  for all the experiments.

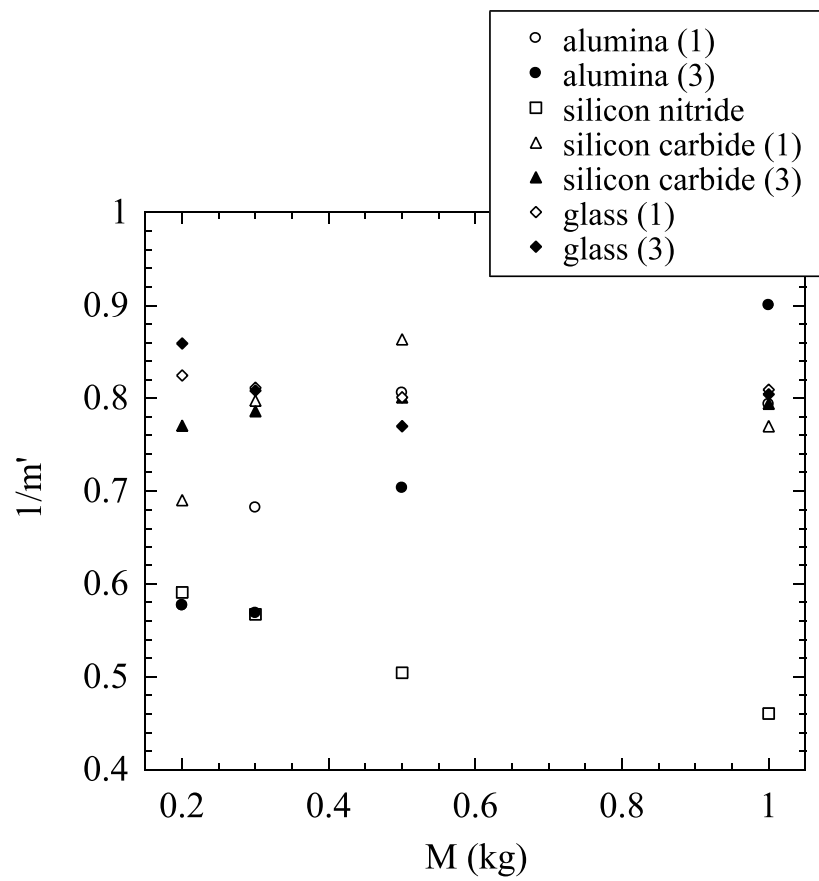


Fig. 18 Change of  $1/m'$  versus applied mass  $M$  for all the experiments.